THE JOURNAL OF PHYSICAL CHEMISTRY B

Article

pubs.acs.org/JPCB

Photodynamics of Free and Solvated Tyrosine

Gaia Tomasello, Matthias Wohlgemuth, Jens Petersen, and Roland Mitrić*

Fachbereich Physik, Freie Universität Berlin, Arnimallee 14, D-14195 Berlin, Germany

Supporting Information

ABSTRACT: We present a theoretical simulation of the ultrafast nonadiabatic photodynamics of tyrosine in the gas phase and in water. For this purpose, we combine our TDDFT/MM nonadiabatic dynamics (Wohlgemuth et al. *J. Chem. Phys.* **2011**, *135*, 054105) with the field-induced surface hopping method (Mitrić et al. *Phys. Rev. A* **2009**, *79*, 053416) allowing us to explicitly include the nonadiabatic effects as well as femtosecond laser excitation into the simulation. Our results reveal an ultrafast deactivation of the initially excited bright $\pi\pi^*$ state by internal conversion to a dark $n\pi^*$ state. We observe deactivation channels along the O−H stretching coordinate as well as involving the N−H bond cleavage of the amino group followed by proton transfer to the phenol ring, which is in agreement with previous static energy path calculations. However, since in the gas phase the canonical form of tyrosine is the most stable one, the proton transfer proceeds in two steps, starting from the carboxyl group that first passes its proton to the amino group, from where it finally moves to the phenol ring. Furthermore, we also investigate the influence of water on the relaxation processes. For the system of tyrosine with three explicit water molecules solvating the amino group, embedded in a classical water sphere, we also observe a relaxation channel involving proton transfer to the phenol ring. However, in aqueous environment, a water molecule near the protonated amino group of tyrosine acts as a mediator for the proton transfer, underlining the importance of the solvent in nonradiative relaxation processes of amino acids.

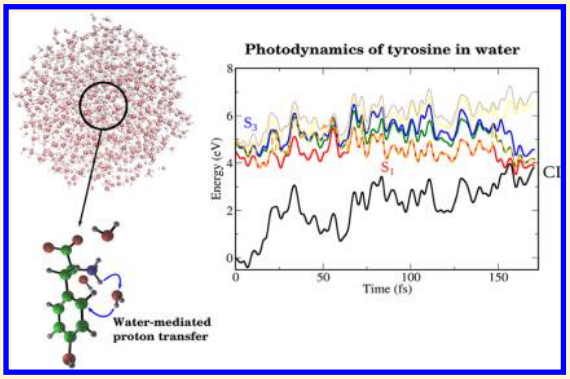

1. INTRODUCTION

Among the vast variety and complexity of biochemical processes, the investigation of the photostability of the building blocks of life such as amino acids and nucleobases is a subject of great importance and intense research. Photostability is governed by the nonradiative relaxation and deactivation occurring upon light irradiation on a femtosecond time scale.[1] The biological molecules found in nature are characterized by the presence of various relaxation pathways that efficiently dissipate the energy gained after UV irradiation to the surrounding environment before any harmful, i.e., irreversible, photoreactions can take place. Of the naturally occurring amino acids, those possessing fluorescent aromatic chromophores, such as tryptophan, tyrosine, and phenylalanine, are mainly responsible for the absorption and fluorescence spectra of proteins,[2] and therefore they are intensively investigated both in gas phase[3] and in solution.[4,5] In particular, tyrosine residues play an important role in enzyme catalysis and have been the focus of extensive investigations. Additionally, since tyrosine is a precursor to dopamine, epinephrine (adrenaline), and other neurotransmitters, it also plays a central role in neurochemistry.

Moreover, due to the fact that the absorption and fluorescence properties of tyrosine are largely influenced by the solvent and neighboring ligands,[6] tyrosine residues can serve as molecular probes for protein solvation and functional electrostatic changes inside proteins. The fluorescence quantum yield of tyrosine, as well as of its chromophore phenol, strongly depends on the excitation wavelength, the temperature, and the pH of the solution. In particular, the fluorescence quantum yield strongly decreases at low pH[7,8] as well as at excitation wavelengths below 245 nm,[9,10] indicating efficient nonradiative processes that must be very fast in order to compete with the fluorescence pathway. Two main fluorescence quenching mechanisms, referred to as external and internal, have been proposed, which both involve a population transfer to the ground state via a conical intersection (CI). The external deactivation channel is the O−H elimination, which has been first revealed by Sobolewski and Domcke on the example of phenol[11,12] and has been attributed to the ubiquitous nature of $\pi\sigma^*$ states that are repulsive along the O−H stretching coordinate.[11] These states exhibit a CI with the lowest bright state of $\pi\pi^*$ character and also with the ground state, leading to ultrafast electronic deactivation. This results in a highly vibrationally excited ground state or, alternatively, in the direct elimination of neutral H atoms as recently observed by time-resolved spectroscopic experiments.[13] In addition, deactivation in amino acids can in general also proceed through decarboxylation and deamination of the side chain.[10,14−17]

However, the experimentally found decrease of the fluorescence lifetimes at low pH, when the amino acids are fully protonated, hints at a different relaxation process, termed

Received: March 6, 2012
Revised: May 25, 2012
Published: June 24, 2012

   dx.doi.org/10.1021/jp302179m | *J. Phys. Chem. B* 2012, 116, 8762−8770

internal quenching, which might be predominantly governed by proton transfer from the protonated amino group. This assumption is supported by minimum energy path calculations of Sobolewski et al. that have revealed the presence of only a small energy barrier (0.1 eV) for the proton transfer from the amino group to the phenol ring.[18] Further indications for such a mechanism can be obtained by comparison with findings on the fluorescence quenching in tryptophan. Recently, Leonard et al.[19] have investigated excited state quenching and photoproduct formation of tryptophan in aqueous solution by performing femtosecond transient absorption experiments. By varying the pH and comparing with the transient spectra of tryptophan incorporated in a peptide, where electron transfer is the dominant quenching mechanism, they could identify a zwitterionic photoproduct with the indole moiety protonated. Formation of this product occurred via excited state proton transfer from the side chain amino group. This has confirmed earlier theoretical predictions obtained by excited state reaction path calculations.[18,20]

From these extensive studies, it can be inferred that electron and proton transfer processes play a key role in the excited state properties of tyrosine. Therefore, a comprehensive investigation of tyrosine photodynamics should not be restricted to the chromophore part of the system (phenol) only, but the side chain as well as all nuclear degress of freedom should be accounted for. Moreover, it can be expected that for tyrosine in solution or in protein environment also neighboring solvent molecules or amino acid residues should affect the photodynamics.

In the present contribution we report for the first time the theoretical investigation of the laser-induced nonadiabatic dynamics of isolated tyrosine including all nuclear degrees of freedom. We confirm the O−H detachment as a deactivation channel in tyrosine. Moreover, we reveal that in the gas phase, the previously predicted proton transfer from the amino group to the phenol ring is preceded by an additional proton transfer step from the carboxyl group to the amino group. Thus, a two-step proton transfer mechanism is identified. Beyond the gas phase study, we have also investigated the nonadiabatic dynamics of tyrosine in water environment in order to shed light on the influence of the solvent. We reveal the presence of a deactivation channel involving proton transfer from the side chain to the chromophore, similar to the finding in the gas phase. In solution, however, the reaction proceeds involving a nearby water molecule which acts as a bridge for the proton transfer.

Our paper is structured in the following way: First, the theoretical approach is outlined in section 2, involving a brief description of the field-induced surface hopping (FISH) method as well as the calculation of the necessary couplings in the framework of time-dependent density functional theory (TDDFT) and the combination of FISH with the quantum mechanical/molecular mechanical (QM/MM) approach. In section 3 the computational details are presented. Subsequently in section 4, the results of our nonadiabatic dynamics simulations on tyrosine are presented and discussed, finally followed by conclusions and outlook in section 5.

2. THEORETICAL FORMULATION

Field-Induced Surface Hopping (FISH). The FISH method is based on the propagation of independent classical trajectories in a manifold of several electronic states under the influence of laser fields with arbitrary shapes. In order to describe the population transfer between these states, which arises both due to the coupling with the laser field and through the intrinsic nonadiabatic coupling, the trajectories are allowed to switch between the states according to quantum mechanically determined probabilities. This is similar to Tully's surface hopping method[21] which is however only suited to describe field-free nonadiabatic transitions in molecular systems.[22−28]

The detailed description of FISH simulations has been already presented in refs 29 and 30. Briefly, the following steps are needed: First, initial conditions for an ensemble of trajectories are generated. Second, along each trajectory which is propagated in the framework of molecular dynamics "on the fly" the electronic degrees of freedom are propagated by solving the time-dependent Schrödinger equation in the manifold of adiabatic electronic states coupled by the laser field $\vec{E}(t)$ and by the nonadiabatic coupling terms $D_{ij}(\mathbf{R}(t)) = \langle \mathbf{\Psi}_i(\mathbf{R}(t)) | (\mathrm{d}\mathbf{\Psi}_j(\mathbf{R}(t))/\mathrm{d}t \rangle$

$$i\hbar \dot{c}_i(t) = E_i(\mathbf{R}(t))c_i(t) - \sum_j [i\hbar D_{ij}(\mathbf{R}(t)) + \vec{\mu}_{ij}(\mathbf{R}(t))\cdot\vec{E}(t)]c_j(t) \quad (1)$$

where $c_i(t)$ are the expansion coefficients of the electronic wave function from which density matrix elements can be calculated as $\rho_{ij} = c_i^* c_j$. Finally, the hopping probabilities are determined in each nuclear time step from the change of the diagonal density matrix elements ρ_{ii}, which correspond to the electronic state populations, according to

$$P_{i\to j} = \Theta(-\dot{\rho}_{ii})\Theta(\dot{\rho}_{jj})\frac{-\dot{\rho}_{ii}}{\rho_{ii}}\frac{\dot{\rho}_{jj}}{\sum_k \Theta(\dot{\rho}_{kk})\dot{\rho}_{kk}}\Delta t \quad (2)$$

where the Θ functions are defined to be one for positive arguments and zero otherwise.[31,32] The hopping probabilities are used in a stochastic process to decide if a state switch occurs. In the absence of a laser field, the total energy of the system during a state switch is conserved by rescaling the nuclear velocities uniformly. If a laser field is present, energy exchange with the molecular system can occur and thus no velocity rescaling is applied. The electronic state population as a function of time is finally obtained by averaging over the ensemble of trajectories.

The above presented FISH method is suitable for the simulation and control of laser-induced processes[29,33] as well as for the simulation of spectroscopic observables such as time-resolved photoelectron spectra[30,34,35] or harmonic emission.[31]

Nonadiabatic Couplings and Transition Dipole Moments in the Framework of TDDFT. The nonadiabatic couplings D_{ij} as well as the transition dipole moments μ_{ij} are obtained from the linear response TDDFT method according to Mitrić et al. by defining an auxiliary wave function for each excited electronic state, consisting of all single excitations in the manifold of the Kohn−Sham (KS) orbitals.[36,37] It has the form

$$|\Psi_i\rangle = \sum_m^{\mathrm{virt}} \sum_n^{\mathrm{occ}} c_{mn}^i(t)\hat{a}_m^\dagger \hat{a}_n |\Phi_{\mathrm{KS}}\rangle \quad (3)$$

where the operator $\hat{a}_m^\dagger$ creates an electron in the virtual orbital m and $\hat{a}_n$ annihilates one in the occupied orbital n, $|\Phi_{\mathrm{KS}}\rangle$ is the ground state KS determinant, and the coefficients c_{mn}^i are determined from the TDDFT eigenvectors.[36] Employing this wave function, the coupling elements are obtained as

dx.doi.org/10.1021/jp302179m | J. Phys. Chem. B 2012, 116, 8762−8770

$$D_{ij} = \langle \Psi_i(t) | \frac{d\Psi_j(t)}{dt} \rangle \approx \frac{1}{2\Delta t}(\langle \Psi_i(t) | \Psi_j(t + \Delta t) \rangle - \langle \Psi_i(t + \Delta t) | \Psi_j(t) \rangle) \quad (4)$$

$$\mu_{ij} = \langle \Psi_i(t) | \hat{\mu} | \Psi_j(t) \rangle \quad (5)$$

Combination of the FISH Nonadiabatic Dynamics with the TDDFT/MM Approach. The extension of nonadiabatic dynamics to the description of systems interacting with their environment in the framework of the quantum mechanical/molecular mechanical (QM/MM) approach has already been presented previously.[38,39] Briefly, the idea of QM/MM is to separate the system into a quantum mechanical part (QM), for which the excited state energies, gradients, and nonadiabatic couplings are calculated quantum mechanically, and a classical part (MM), which is treated using common force field methods. In the most straightforward mechanical embedding approach, which has been employed in the present work, the interaction of the QM and MM regions is restricted to the steric repulsion between solvent and solute, and the Hamiltonian of the QM system is not directly affected by the MM environment. Therefore, polarization effects from the solvent environment on the QM wave function are not included in this model. However, in our case we treat the most important solvent molecules explicitly as parts of the QM system, hence taking into account their interaction with the solute molecule without further approximations. This allows us to realistically model the solute−solvent interaction in the region of interest for the photodynamical processes under study while retaining a simplified description of the remaining solvent molecules.

In the case that both the QM part (X) and the MM part (Y) are sufficiently well described by the classical force fields, the effect of sterical repulsion between them can be calculated as the difference between the MM energy of the combined system (X + Y) and the QM system alone. The total energy of the combined system in the frame of QM/MM approach can then be written as:

$$E_{QM+MM} = E_{QM}(X) + [E_{MM}(X + Y) - E_{MM}(X)] \quad (6)$$

The forces needed to carry out dynamics "on the fly" are obtained as the gradient of eq 6 and the nonadiabatic couplings are calculated only for the QM part.

3. COMPUTATIONAL METHODS

The structure of isolated tyrosine has been optimized using density functional theory (DFT) employing the PBE0 functional[40] and the TZVP basis set[41] as implemented in TURBOMOLE.[42] For the dynamics simulations, the electronic structure was described in the framework of time-dependent density functional theory (TDDFT) using the PBE0 functional and the smaller SV(P) basis set.[43,44] This allows for a more efficient computation of the needed energies and gradients while giving only minor deviations to the results obtained with the TZVP basis set, as has been examined by comparing the absorption spectra and a limited number of nonadiabatic reference trajectories. Furthermore, the position and character of the lowest-lying excited states are also reproduced at higher levels of theory (CAM-B3LYP[45]/SVP, CAM-B3LYP/TZVP, and CC2[46]/TZVP) as discussed in the Supporting Information, Table S1.

The 60 initial coordinates and momenta have been generated by propagating a trajectory in the electronic ground state at constant temperature (298 K) for 10 ps and then sampling the structures each 100 fs.

For the propagation of the nuclei, the Newtonian equations of motion have been integrated using the velocity Verlet[47] algorithm with a time step of 0.1 fs. Along each trajectory, the electronic Schrödinger equation (1) has been integrated using the fourth order Runge−Kutta method with a time step of 10^{-5} fs.

In order to simulate the excitation by a laser field, the system has been excited resonantly to the most intensive electronic transition by a Gaussian pump laser pulse of the form

$$E(t) = E_0 \exp\left(-\frac{(t - t_0)^2}{2\sigma^2}\right) \sin \omega(t - t_0) \quad (7)$$

The ensemble of trajectories was propagated in the manifold of the ground state and the six lowest excited singlet states including both the interaction with the laser field as well as nonadiabatic effects. The explicit inclusion of the pump pulse allows us to more realistically model the experimental excitation process leading to a population of several excited electronic states. As discussed in section 2 no velocity rescaling is applied after a hopping event during the action of the pulse, since the interaction between molecule and laser field implies the nonconservation of the molecular energy. For times larger than the 2 σ width of the Gaussian pulse ($t_0 \pm 2\sigma$), when the field strength is negligible, the velocity rescaling is enabled and field-free nonadiabatic dynamics with conserved total energy is carried out. In this way the electronic relaxation dynamics after initial excitation is described analogously to the purely field-free nonadiabatic dynamics. The difference of both approaches lies in the initial excitation, which is in the field-free case simplified by starting all trajectories directly in the desired excited state which exhibits the highest oscillator strength.

In order to explore the photodynamics of solvated tyrosine we have considered also the molecule surrounded by water. Under these conditions, tyrosine is most stable in the zwitterionic form. The model for the solvated tyrosine has been obtained by embedding it in a 49 Å cubic water box followed by equilibration using force field molecular dynamics under periodic boundary conditions over 100 ps at a pressure of 1.0 bar and a temperature of 300 K employing the TINKER program.[48] For tyrosine, the OPLS-AA[49−51] and for water the TIP-3P[52] force field were used. After equilibration, a sphere of 21 Å radius, including tyrosine and 1268 water molecules, was cut from the box and further relaxed using the QM/MM approach for 3 ps at 300 K. The QM part consisted of the tyrosine molecule only, which was described by DFT employing the PBE0 functional and the SV(P) basis set. From this QM/MM trajectory, the initial conditions for the nonadiabatic dynamics simulations were generated by sampling at regular time intervals. In order to obtain an almost spherical water droplet, the water spheres of each initial condition have been further truncated to 20 Å. For taking into account the interaction between the solvent and the polar amino group of tyrosine explicitly, the QM part of the system was extended to include also the three water molecules situated most closely to the amino group. This allowed us to investigate also the influence of hydrogen bonding at the amino group on the relaxation dynamics. Since for the zwitterionic tyrosine in water the presence of charge-transfer excitations can be expected, the

dx.doi.org/10.1021/jp302179m | J. Phys. Chem. B 2012, 116, 8762−8770

electronic structure was described using the Coulomb-attenuated B3-LYP functional (CAM-B3LYP)[45] together with the SVP basis set,[43,44] as implemented in the Gaussian 09 program suite.[53] This functional has been developed in order to improve the description of long-range charge transfer transitions. The position and character of the lowest-lying excited states have been validated against higher level calculations (CAM-B3LYP/SVP, CAM-B3LYP/TZVP, and CC2/TZVP) as discussed in the Supporting Information, Table S2. Due to the much higher computational cost employing the CAM-B3LYP functional, only a limited number of trajectories has been propagated.

4. RESULTS AND DISCUSSION

Ultrafast Relaxation of Isolated Tyrosine: Nonadiabatic and Laser-Induced Dynamics. Since in the gas phase the canonical form of tyrosine is more stable than the zwitterionic one, the former has been considered for the gas phase simulation of the present contribution. Among the several low-lying conformers,[54] we have selected the one shown in Figure 1. The electronic absorption spectra for the optimized ground state structure of tyrosine in the gas phase as well as for the whole initial thermal 300 K ensemble of 60 structures obtained with TDDFT [PBE0/SV(P)] are shown in Figure 1. In agreement with experimental data,[3] the spectrum is characterized by two bands at wavelengths above 200 nm corresponding to two $\pi\pi^*$ transitions usually labeled as L_a and L_b according to the Platt notation. The lower-lying state is located at 244 nm (5.07 eV) and the second one at 210 nm (5.89 eV), corresponding to a slight blue shift compared to the experiment, where the first absorption band is situated between 260 and 280 nm (4.77−4.43 eV) and the second, more intense one at 220 nm (5.64 eV), respectively.[3] At the equilibrium geometry (cf. Figure 1b), the two lowest-lying bright states are S_1 and S_3 which both have $\pi\pi^*$ character. The S_1 state can be identified with the less intensive L_b state which is more stable in the gas phase, while S_3 corresponds to L_a, the more intensive state with higher permanent dipole moment. Between these bright states, an additional dark state is found (S_2), which is characterized by orbital excitations within the amino and carboxyl groups. These findings are reproduced at higher levels of theory using the larger TZVP basis set, the range-separated CAM-B3LYP functional as well as the coupled cluster approach CC2 as pointed out in the Supporting Information, Table S1. Moreover, also the results of Sobolewski et al. on tyrosine +2 H_2O at the CC2 level show a similar character of the first three excited states (ref 17, cf. also the Supporting Information). The higher-lying states S_6 and S_{10} are repulsive and are mainly important for the deactivation channels observed during the nonadiabatic dynamics. Specifically, S_6 has $\pi\sigma^*$ character and is repulsive along the O−H stretching coordinate, while S_{10} is the repulsive $\pi\sigma^*$ state located on the N−H stretching coordinate.

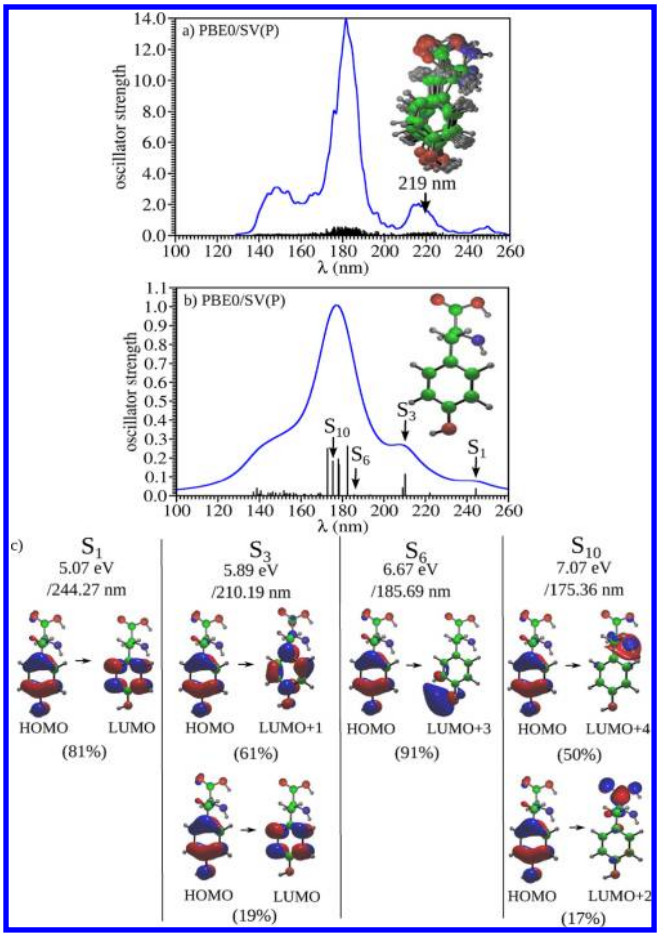

Figure 1. Electronic absorption spectra of isolated tyrosine including the lowest 40 excited singlet states obtained by TDDFT [PBE0/SV(P)] for the thermal ensemble of 60 structures at 300 K (a) and for the equilibrium geometry (b). The individual transitions (black sticks) have been convoluted by a Lorentzian width of 2 nm (blue lines) for the spectrum of the ensemble and by a Lorentzian width of 20 nm for the spectrum of the equilibrium structure. Panel c shows the character of the most relevant singlet states in terms of the leading orbital excitations.

For comparison, we show in Figure 2 the absorption spectrum obtained using the more accurate CAM-B3LYP functional. Overall, the spectrum is quite similar to the one shown in Figure 1, in particular regarding the character and the position of the two $\pi\pi^*$ states S_1 and S_3. However, there is less splitting between the higher states, such that the lowest-lying repulsive state of $\pi\sigma^*$ character corresponds already to S_4 at CAM-B3LYP/SVP level.

In order to study the photodynamics of tyrosine we have performed nonadiabatic molecular dynamics simulations in the manifold of the ground state and the lowest six excited singlet states. We have first propagated the ensemble of trajectories starting directly from the bright state S_3 without including the excitation field. Subsequently, also FISH simulations directly accounting for the field-induced excitation have been carried out.

The nonadiabatic dynamics started in the S_3 state is characterized by ultrafast population transfer via the S_2 to the S_1 state with an S_3 lifetime of 11.8 fs, as shown in Figure 3. The maximal S_1 population of ∼60% is reached after 30 fs, followed by slow decay to the ground state. After the total propagation time of 200 fs, about 10% of the trajectories have returned to the ground state. This occurs via an efficient reactive channel characterized by a double proton transfer process (see Figure 4) which drives the system toward a low-lying conical intersection between the S_1 and S_0 states. The degeneracy is induced by an out-of-plane bending of an aromatic carbon in the phenyl ring at the C1 or C2 position, respectively. The major part of the trajectories, however, remains trapped in the S_1 state until the end of the simulation.

During the internal conversion from S_3 to S_2 and S_1, in most cases the electronic state character changes from $\pi\pi^*$ to $n\pi^*$,

dx.doi.org/10.1021/jp302179m | J. Phys. Chem. B 2012, 116, 8762−8770

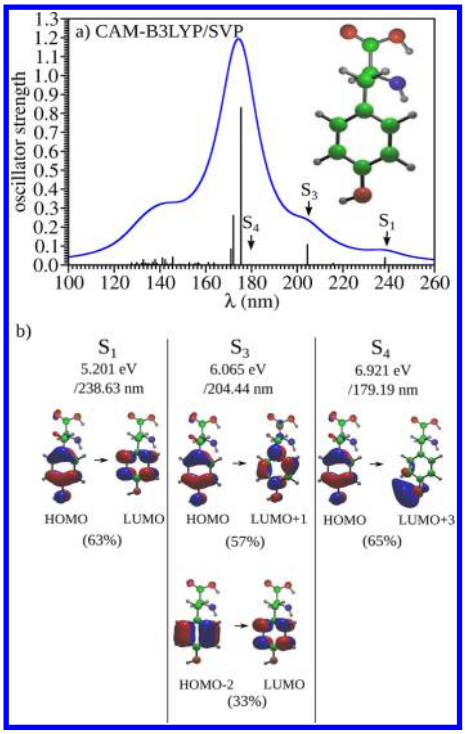

Figure 2. Electronic absorption spectrum of isolated tyrosine including the lowest 40 excited singlet states obtained by TDDFT (CAM-B3LYP/SVP) for the equilibrium geometry optimized at the same level (a). The individual transitions (black sticks) have been convoluted by a Lorentzian width of 20 nm (blue line). Panel b shows the character of the most relevant singlet states in terms of the leading orbital excitations.

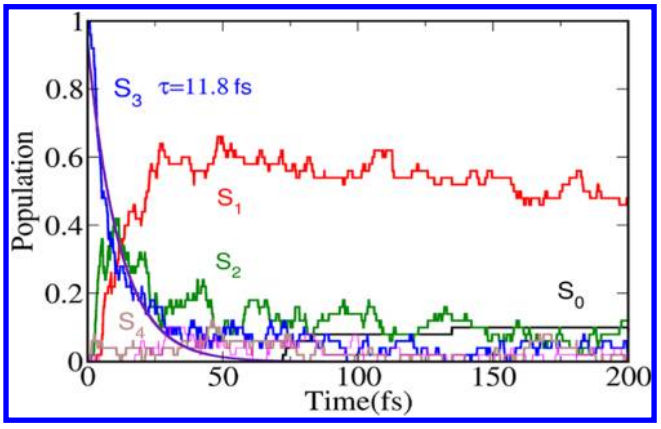

Figure 3. Time-dependent electronic state populations of isolated tyrosine during the field-free nonadiabatic dynamics employing TDDFT [PBE0/SV(P)]. The violet line represents an exponential fit to the population of the state S_3 with a lifetime τ of 11.8 fs.

which is accompanied by a structural rearrangement from the neutral to the zwitterionic form of tyrosine. At this stage the molecule is prearranged for the proton transfer to the phenol ring, where charge density may be accumulated in agreement with the previously proposed H-acceptor model.[20] In previous theoretical investigations using the coupled cluster method CC2, the proton transfer pathway to the phenol ring was found to exhibit a small barrier of 0.1 eV,[18] whereas in our TDDFT calculations this path is even barrierless. Concerning the distribution of charges during the process, it is still an open question if the H transfer is nucleophilic or electrophilic.

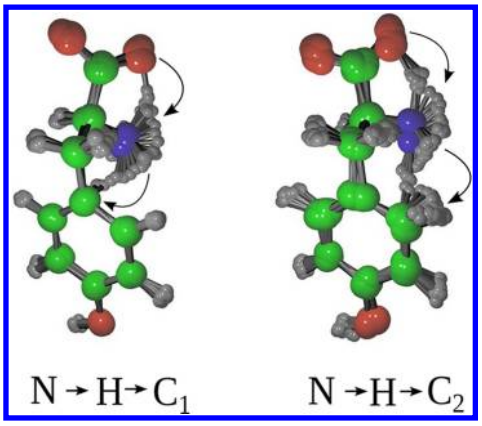

Figure 4. Illustration of the proton transfer from the carboxyl and amino groups to the carbon atoms C1 (left) and C2 (right). For both processes, snapshots of a representative trajectory are superimposed for every 0.5 fs of the relevant part of the dynamics.

Therefore, we have performed a Mulliken population analysis which has revealed a positive charge accumulation at the migrating H and a negative one at the accepting phenol carbon, confirming the electrophilic nature of the process.

Among all of the reactive trajectories, the proton transfer pathways from the amino group to C1 and to C2 have been observed with equal incidence (see Figure 4). Although the C2 position is sterically favored, the C1 position is also an efficient reaction site due to the electron-donating effect induced by the OH group in para position.

Remarkably, for one reactive trajectory a decarboxylation process has been observed after the decay to S_0, giving rise to a bicyclic photoproduct (cf. Figure 5). From the experimental side, there is no data available for photoinduced decarboxylation in tyrosine. However, in the case of tryptophan the deacarboxylation quantum yield has been determined to 0.8%,[55] indicating that such a process is present as a minor reaction channel.

In order to study the role the laser-induced electronic excitation plays in the nonadiabatic dynamics of tyrosine, also simulations using the FISH method have been performed, using the same set of 60 initial conditions as in the field-free case. For the excitation a Gaussian pump pulse has been employed (see eq 7), with the amplitude $E_0 = 0.01E_h/(ea_0)$ corresponding to an intensity of 3.5×10^{12} W/cm^2, a frequency $\omega_{pump} = 5.66$ eV (219 nm) resonant to the bright state S_3, a temporal width of 23.5 fs ($\sigma = 10$ fs) and $t_0 = 20$ fs. As shown in Figure 6, this pulse leads to photoexcitation of about 90% of the trajectories, mainly to the S_3 state, but also to S_2 and S_4. The initial excitation is rapidly followed by internal conversion to the S_1 state after the pulse has ceased. Within 100 fs, almost the total excited state population is transferred to S_1. Subsequently, a slow decay to the ground state is present, which is reached by 17% of the initially excited trajectories after 200 fs.

Compared to the field-free dynamics, the FISH simulation gives rise to a larger number of possible reaction channels for the nonadiabatic deactivation to the ground state. The main pathway is the pure H abstraction from the protonated amino group, which is occasionally followed by proton transfer to the phenol ring.

A more detailed insight into this process responsible for the internal fluorescence quenching can be gained by analyzing the selected nonadiabatic trajectory shown in Figure 7. In this case, at ~14 fs the pump pulse transfers the trajectory to the bright

dx.doi.org/10.1021/jp302179m | J. Phys. Chem. B 2012, 116, 8762−8770

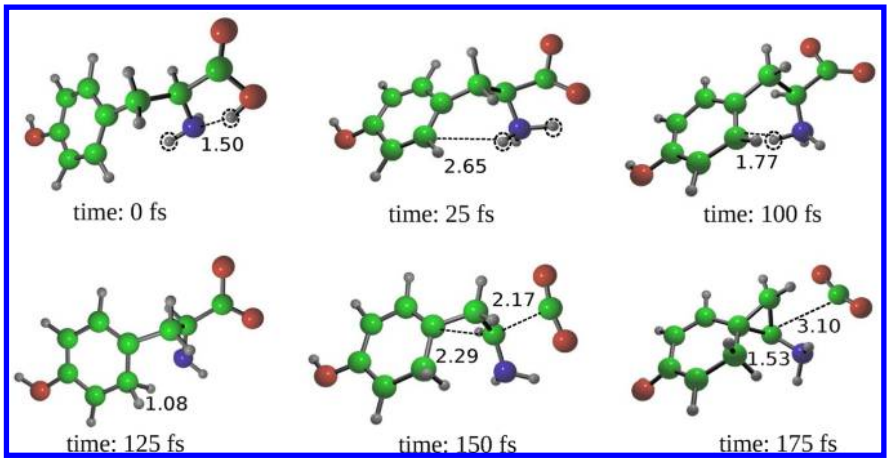

Figure 5. Snapshots of a nonadiabatic trajectory showing decarboxylation of tyrosine. At 25 fs the proton transfer from the carboxyl to the amino group occurs. Subsequently, after 125 fs the phenol C2 atom has been protonated, and the decay to the ground state through a CI is observed. This is finally followed by decarboxylation (CO_2 formation) and the formation of a bicyclic photoproduct after 175 fs. The atom distances and bond lengths are given in Å.

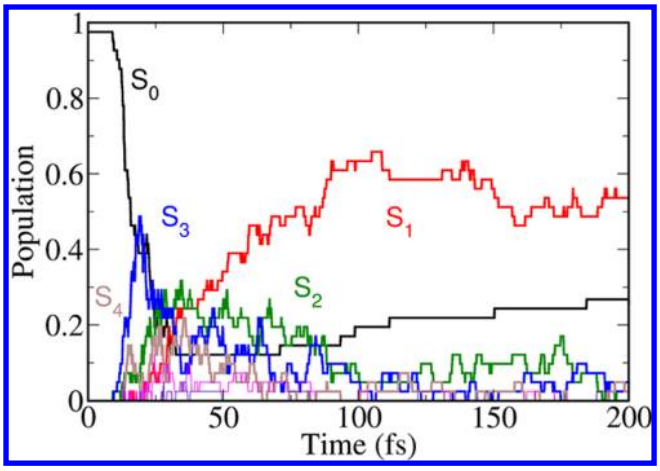

Figure 6. Time-dependent electronic state populations in isolated tyrosine employing FISH nonadiabatic dynamics combined with TDDFT [PBE0/SV(P)]. The excitation is due to a resonant 219 nm pulse with a width of 23.5 fs.

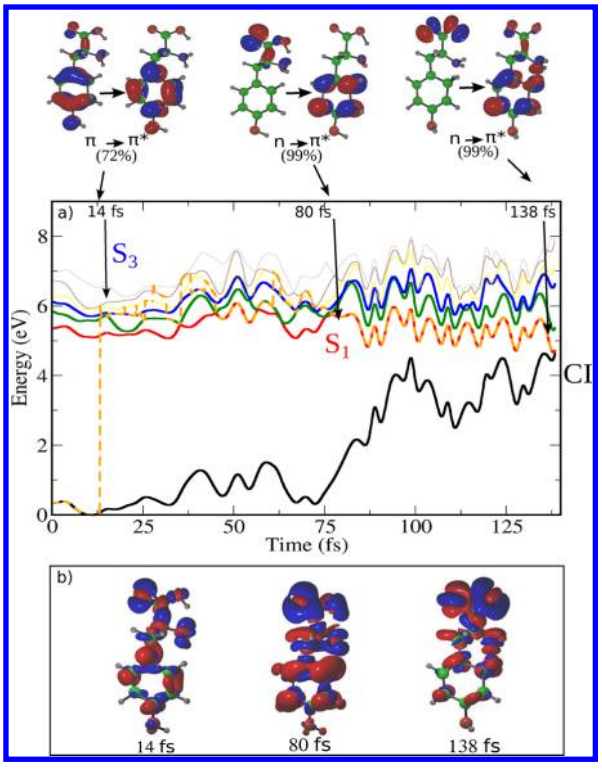

Figure 7. (a) Relative energies of the lowest 6 electronic states obtained by TDDFT [PBE0/SV(P)] along a selected nonadiabatic trajectory where the protonation of the chromophore has been observed as deactivation channel. The actual state in which the trajectory resides is labeled by the orange dashed line. For selected time steps, the character of this state is illustrated on the top of panel a by the main orbital excitations and in panel b by the electron density difference to the ground state.

state S_3, which is of mixed $\pi\pi^*/n\pi^*$ character (with the n orbital localized on the carboxyl group and the π^* orbital on the phenol ring). Within 75 fs the relaxation proceeds to the S_1 state with $n\pi^*$ character. In this state, the proton transfer from the carboxyl group to the amino group takes place, followed by the stretching of one N−H bond. As the dynamics proceeds toward a conical intersection with the ground state, the proton transfer to the phenol ring occurs, and the ground state is reached after ∼140 fs.

Interestingly, within the FISH simulations an additional deactivation channel has been observed, as illustrated for a selected trajectory in Figure 8. Here, the dynamics proceeds mostly in the higher excited states S_2 to S_5, and the final return to the S_1 state does not take place before ∼140 fs. At this time, the S_1 state is of $\pi\sigma^*$ character. The subsequent dynamics is straightforwardly directed toward a conical intersection with the ground state which is reached at 150 fs. This is accompanied by a strong excitation of the O−H stretching vibration, ultimately leading to the breaking of the O−H bond as can be recognized from the time-dependent bond distances shown in Figure 8b. These findings are in agreement with the model by Sobolewski and Domcke, who have identified the O−H detachment as a feasible relaxation mechanism induced by $\pi\pi^*/\pi\sigma^*$ internal conversion and therefore population of a $\pi\sigma^*$ state which is repulsive along the O−H stretching coordinate.[11−13] Experimental evidence for this process has been recently provided by Stavros et al.[13] who have observed H atom elimination through $\pi\sigma^*$ states after excitation at 200 nm. The occurrence of this deactivation channel only within the FISH dynamics

dx.doi.org/10.1021/jp302179m | J. Phys. Chem. B 2012, 116, 8762−8770

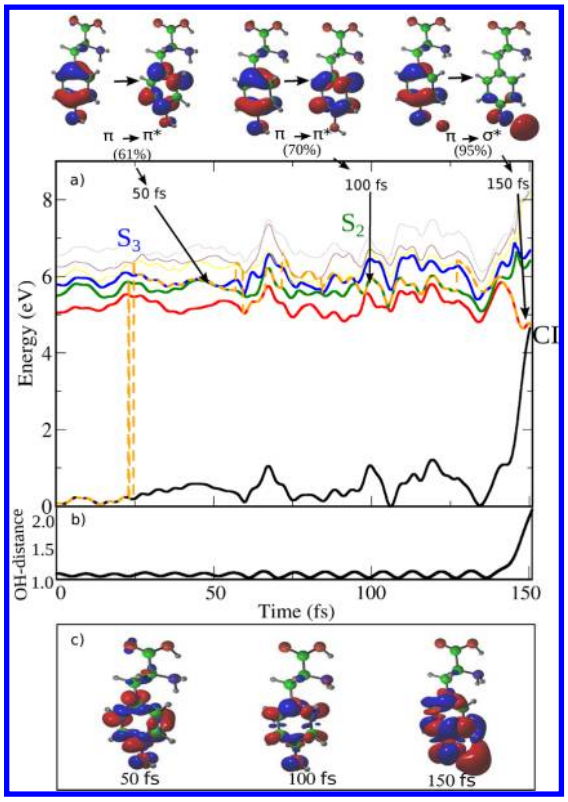

Figure 8. Relative energies of the lowest 6 electronic states obtained by TDDFT [PBE0/SV(P)] along a selected nonadiabatic trajectory where the O−H detachment has been observed as deactivation channel. The actual state in which the trajectory resides is labeled by the orange dashed line. For selected time steps, the character of this state is illustrated on the top of panel a by the main orbital excitations and in panel c by the electron density difference to the ground state. The inset (panel b) shows the temporal evolution of the O−H bond distance in Å along the trajectory.

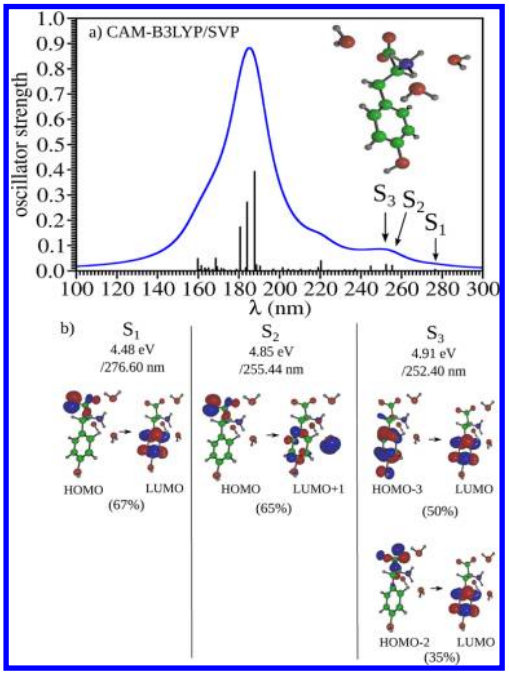

Figure 9. Electronic absorption spectrum of tyrosine with three explicit water molecules embedded in a classical water sphere, calculated with TDDFT [CAM-B3LYP/SVP]. The individual transitions (black sticks) have been convoluted by a Lorentzian width of 20 nm (blue line). Panel b shows the character of the first three excited states S_1, S_2, and S_3 in terms of the leading orbital excitations.

simulations but not within the field-free nonadiabatic dynamics underlines the need for a correct description of the electronic excitation in order to realistically simulate the photodynamical processes.

The character of the near-degeneracies between the S_1 and S_0 states involved in both relaxation channels has been carefully examined, due to the known deficiency of linear response TDDFT in properly describing conical intersections. Employing the complete active space self-consistent field method (CASSCF),[56,57] the presence of small energy gaps has been confirmed as shown in the Supporting Information, Table S3, indicating that the respective TDDFT geometries lie indeed close to a conical intersection.

Ultrafast Dynamics of Microsolvated Tyrosine. In order to investigate the influence of water environment on the dynamical properties and the relaxation channels, we have carried out nonadiabatic dynamics simulations in the framework of QM/MM, where the QM system consisted of tyrosine in the zwitterionic form and three water molecules solvating the protonated amino group. The remaining water environment was described by a classical force field interacting with the QM part using the mechanical embedding scheme. For the electronic structure of the QM system the CAM-B3LYP functional was employed in order to achieve a realistic description of the charge transfer excitations present in polar solvents. The experimental absorption spectrum of tyrosine in water is characterized by two intense peaks at 225 (5.51 eV) and 282 nm (4.39 eV)[5] which have been identified with the L_a and L_b bands. The theoretical spectrum of tyrosine + $3H_2O$ obtained with TDDFT (CAM-B3LYP/SVP) is shown for a selected geometry in Figure 9. This geometry has not been optimized but corresponds to the initial conditions of the nonadiabatic trajectory which will be discussed below. The spectrum exhibits the first transition of $\pi\pi^*$ character at 252 nm, which corresponds to the S_3 state. The lower-lying states have less intensity and are of $n\pi^*$ (S_1) and charge transfer to solvent (CTTS) character (S_2). It should be noticed, that the character and position of the excited states depends strongly on the chosen geometry of tyrosine as well as on the position of the explicit water molecules. In order to validate the chosen computational approach, we have calculated the absorption spectrum for the given structure also at higher computational level employing TDDFT with larger basis sets as well as the coupled cluster method CC2. These calculations are presented in the Supporting Information, Table S2, and show only minor differences to the spectrum shown in Figure 9. According to the electronic state character, the S_3 state was subsequently chosen as initial state for the nonadiabatic dynamics simulations.

Due to the considerable computational cost of calculations using the CAM-B3LYP functional, only a limited number of trajectories has been employed in the nonadiabatic dynamics simulations involving the ground and the 5 lowest excited singlet states. Among a total of 5 trajectories, in one case the nonadiabatic decay involving a proton transfer process is observed. In contrast to the gas phase, in solution a water molecule acts as a bridge for the proton migration, leading to a two-step mechanism which is analyzed in terms of energies and

dx.doi.org/10.1021/jp302179m | J. Phys. Chem. B 2012, 116, 8762−8770

electronic state character in Figure 10, whereas the structural rearrangement is illustrated by the snapshots shown in Figure 11.

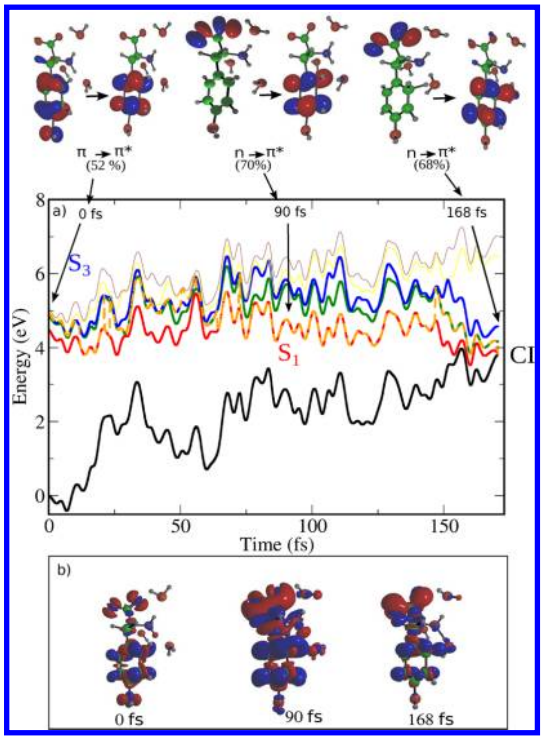

Figure 10. Relative energies of the lowest five electronic states obtained by TDDFT [CAM-B3LYP/SVP] along a selected nonadiabatic trajectory of tyrosine +3 H_2O in a classical water sphere. The actual state in which the trajectory resides is labeled by the orange dashed line. For selected time steps, the character of this state is illustrated on the top of panel a by the main orbital excitations and in panel b by the electron density difference to the ground state.

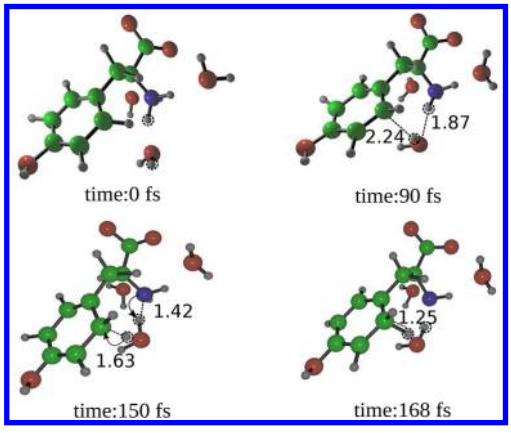

Figure 11. Snapshots of a selected nonadiabatic trajectory of tyrosine in water, showing the double proton transfer mechanism for nonadiabatic decay. At 150 fs the zwitterionic isomer of tyrosine transfers a proton from the amino group to a neighboring water molecule. From there, the proton is further passed to the C2 atom of the phenol ring, and the decay to the ground state occurs after 168 fs. The atom distances and bond lengths are given in Å.

Starting in the $\pi\pi^*$ S_3 state, the trajectory reaches the first excited state, which has then $n\pi^*$ character, after 60 fs. Within the following ~90 fs, the water molecules near the amino group are prearranged as to enable the proton transfer (cf. Figure 11). The latter takes place within the next 20 fs, in which almost simultaneously one proton is donated from the amino group to the nearest water molecule, and another one from the water molecule to the C2 carbon of the phenol ring. Subsequently the decay to the ground state occurs after ~170 fs through to the same "benzene-kink" conical intersection as in the gas phase.

These findings confirm the presence of an "internal" deactivation channel for tyrosine photoreactivity also in a polar solvent. In contrast to the gas phase, neighboring solvent molecules play a decisive role by mediating the proton transfer from the side chain to the phenol ring. This emphasizes the need to introduce explicit water molecules for a correct description of the electrophilic proton addition to the chromophore and therefore of the ultrafast nonradiative decay of tyrosine in water.

5. CONCLUSIONS

We have presented the investigation of nonadiabatic photodynamics of tyrosine in the gas phase and in water. The gas phase dynamics has been explored by a combination of nonadiabatic molecular dynamics "on the fly" with time-dependent density functional theory. Both the field-free nonadiabatic relaxation as well as the laser field-induced dynamics in the framework of the FISH method have been simulated. We have shown that after initial excitation to the bright $\pi\pi^*$ states ultrafast internal conversion occurs to the lowest excited singlet state, which has mainly $n\pi^*$ character at this stage of the dynamics. Subsequently, nonradiative relaxation to the ground state can occur through conical intersections. Beyond the well-known deactivation channel via O−H bond breaking in repulsive $\pi\sigma^*$ states, also the transfer of a proton from the side chain to the phenol ring represents an efficient deactivation path. In the gas phase, where the canonical form of tyrosine is the most stable one, this involves a two-step mechanism: The carboxyl group of the side chain first passes its proton to the amino group, from which it further migrates to the phenol ring. This is accompanied by efficient fluorescence quenching, as radiationless decay from S_1 to S_0 occurs through a conical intersection. The degeneracy in this case is induced by an out-of-plane bending of the aromatic carbon atom (C1 or C2) which is being protonated.

Beyond the gas phase study, we have also investigated the influence of solvent environment on the photodynamics of tyrosine by utilizing the combination of our TDDFT-nonadiabatic dynamics approach with the QM/MM technique. Specifically, the zwitterionic conformer of tyrosine together with three explicit water molecules has been embedded in a classical water sphere of 20 Å radius, and the nonadiabatic relaxation has been simulated. The relaxation mechanism found in this way is analogous to the one observed in the gas phase as it also involves transfer of a proton from the side chain to the phenol ring. However, in this case in the first step a proton is donated from the protonated amino group to a nearby water molecule, which acts as a mediator and subsequently passes the proton to the phenol ring. This emphasizes the decisive role of water in the photodynamics of tyrosine.

■ ASSOCIATED CONTENT

Supporting Information

For validation of the results presented above, the energies and oscillator strengths of the first six excited electronic states are provided for isolated tyrosine in Table S1 as well as for tyrosine + 3H_2O in Table S2, employing TDDFT with larger basis sets

dx.doi.org/10.1021/jp302179m | J. Phys. Chem. B 2012, 116, 8762−8770

as well as the linear response coupled cluster method CC2. Furthermore, the near-degeneracies at the last points of the trajectories analyzed in Figures 7 and 8 are validated by comparing them with the energy gaps at the CASSCF level as shown in Table S3. This material is available free of charge via the Internet at http://pubs.acs.org.

AUTHOR INFORMATION

Corresponding Author

*E-mail: mitric@zedat.fu-berlin.de.

Notes

The authors declare no competing financial interest.

ACKNOWLEDGMENTS

We acknowledge financial support from the Deutsche Forschungsgemeinschaft, FOR 1282 (J.P. and R.M.), SPP 1391 (R.M.), and Emmy Noether Program (MI-1236) (R.M. and M.W.). In addition, G.T. thanks the Alexander von Humboldt Foundation (Grant Card. No. 7000260646) for financial support.

REFERENCES

(1) Zewail, A. H. *J. Phys. Chem. A* **2000**, *104*, 5660−5694.
(2) Konev, S. V. *Fluorescence and Phosphorescence of Proteins and Nucleic Acids*; Plenum: New York, 1967.
(3) Zhang, J. Y.; Nagra, S.; Li, L. *Anal. Chem.* **1991**, *63*, 2995−2999.
(4) Wetlaufer, D.; Edsall, J.; Hollingworth, B. *J. Biol. Chem.* **1958**, *233*, 1421−1428.
(5) Truong, T.; Petit, A. *J. Phys. Chem.* **1979**, *83*, 1300−1305.
(6) Ross, T.; Lee, J. *J. Phys. Chem. B* **1998**, *102*, 4612−4618.
(7) Audrey, W. *Biochem. J.* **1971**, *71*, 217−220.
(8) Guzow, K.; Szabelski, M.; Rzeska, A.; Karolczak, J.; Sulowska, H.; Wiczk, W. *Chem. Phys. Lett.* **2002**, *362*, 519−526.
(9) Köhler, G.; Getoff, N. *Chem. Phys. Lett.* **1974**, *26*, 525−528.
(10) Creed, D. *Photochem. Photobiol.* **1984**, *39*, 563−575.
(11) Sobolewski, A. L.; Domcke, W.; Dedonder-Lardeaux, C.; Jouvet, C. *Phys. Chem. Chem. Phys.* **2002**, *4*, 1093−1100.
(12) Lan, Z. G.; Domcke, W.; Vallet, V.; Sobolewski, A.; Mahapatra, S. *J. Chem. Phys.* **2005**, *122* (Article 224315), 1−13.
(13) Iqbal, A.; Stavros, V. G. *J. Phys. Chem. Lett.* **2010**, *1*, 2274−2278.
(14) Holt, L. A.; Milligan, B.; Rivett, D. E.; Stewart, F. H. *Biochim. Biophys. Acta* **1977**, *499*, 131−138.
(15) Dillon, J. *Photochem. Photobiol.* **1980**, *32*, 37−39.
(16) Beechem, J. M.; Brand, L. *Annu. Rev. Biochem.* **1985**, *54*, 43−71.
(17) Sobolewski, A.; Shemesh, D.; Domcke, W. *J. Phys. Chem. A* **2009**, *113*, 542−550.
(18) Gregoire, G.; Jouvet, C.; Dedonder, C.; Sobolewski, A. *J. Am. Chem. Soc.* **2006**, *129*, 6223−6231.
(19) Leonard, J.; Sharma, D.; Szafarowicz, B.; Torgasin, K.; Haacke, S. *Phys. Chem. Chem. Phys.* **2010**, *12*, 15744−15750.
(20) Blancafort, L.; Gonzalez, D.; Olivucci, M.; Robb, M. A. *J. Am. Chem. Soc.* **2002**, *124*, 6398−6406.
(21) Tully, J. C. *J. Chem. Phys.* **1990**, *93*, 1061−1071.
(22) Mitrić, R.; Bonačić-Koutecký, V.; Pittner, J.; Lischka, H. *J. Chem. Phys.* **2006**, *125* (Article 024303), 1−7.
(23) Tapavicza, E.; Tavernelli, I.; Rothlisberger, U. *Phys. Rev. Lett.* **2007**, *98* (Article 023001), 1−4.
(24) Barbatti, M.; Granucci, G.; Persico, M.; Ruckenbauer, M.; Vazdar, M.; Eckert-Maksić, M.; Lischka, H. *J. Photochem. Photobiol. A.: Chem.* **2007**, *190*, 228−240.
(25) Fabiano, E.; Thiel, W. *J. Phys. Chem. A* **2008**, *112*, 6859−6863.
(26) Barbatti, M.; Lischka, H. *J. Am. Chem. Soc.* **2008**, *130*, 6831−6839.
(27) Lan, Z.; Fabiano, E.; Thiel, W. *J. Phys. Chem. B* **2009**, *113*, 3548−3555.
(28) Vazdar, M.; Eckert-Maksić, M.; Barbatti, M.; Lischka, H. *Mol. Phys.* **2009**, *107*, 845−854.
(29) Mitrić, R.; Petersen, J.; Bonačić-Koutecký, V. *Phys. Rev. A* **2009**, *79* (Article 053416), 1−6.
(30) Mitrić, R.; Petersen, J.; Wohlgemuth, M.; Werner, U.; Bonačić-Koutecký, V.; Wöste, L.; Jortner, J. *J. Phys. Chem. A* **2011**, *115*, 3755−3765.
(31) Lisinetskaya, P. G.; Mitrić, R. *Phys. Rev. A* **2011**, *83* (Article 033408), 1−13.
(32) Mitrić, R.; Petersen, J.; Bonačić-Koutecký, V.Multistate Nonadiabatic Dynamics 'on the fly"in Complex Systems and Its Control by Laser Fields. In *Conical Intersections - Theory, Computation and Experiment*; Domcke, W., Yarkony, D. R., Köppel, H., Eds.; Advanced Series in Physical Chemistry Vol. 17; World Scientific: Singapore, 2011.
(33) Petersen, J.; Mitrić, R.; Wolf, J. P.; Roslund, J.; Bonačić-Koutecký, V.; Rabitz, H. *Phys. Rev. Lett.* **2010**, *105* (Article 073003), 1−4.
(34) Mitrić, R.; Petersen, J.; Wohlgemuth, M.; Werner, U.; Bonačić-Koutecký, V. *Phys. Chem. Chem. Phys.* **2011**, *13*, 8690−8696.
(35) Stanzel, J.; Neeb, M.; Eberhardt, W.; Lisinetskaya, P. G.; Petersen, J.; Mitrić, R. *Phys. Rev. A* **2012**, *85* (Article 013201), 1−6.
(36) Mitrić, R.; Werner, U.; Bonačić-Koutecký, V. *J. Chem. Phys.* **2008**, *129* (Article 164118), 1−9.
(37) Werner, U.; Mitrić, R.; Bonačić-Koutecký, V. *J. Chem. Phys.* **2010**, *132* (Article 174301), 1−8.
(38) Wohlgemuth, M.; Mitrić, R.; Bonačić-Koutecký, V. *J. Chem. Phys.* **2011**, *135* (Article 054105), 1−10.
(39) Petersen, J.; Wohlgemuth, M.; Sellner, B.; Bonačić-Koutecký, V.; Lischka, H.; Mitrić, R. *Phys. Chem. Chem. Phys.* **2012**, *14*, 4687−4694.
(40) Adamo, C.; Barone, V. *J. Chem. Phys.* **1999**, *110*, 6158−6171.
(41) Schäfer, A.; Huber, C.; Ahlrichs, R. *J. Chem. Phys.* **1994**, *100*, 5829−5836.
(42) Ahlrichs, R.; Bär, M.; Haser, M.; Horn, H.; Kolmel, C. *Chem. Phys. Lett.* **1989**, *162*, 165−169.
(43) Schäfer, A.; Horn, H.; Ahlrichs, R. *J. Chem. Phys.* **1992**, *97*, 2571−2578.
(44) Weigend, F.; Ahlrichs, R. *Phys. Chem. Chem. Phys.* **2005**, *7*, 3297−3305.
(45) Yanai, T.; Tew, D.; Handy, N. *Chem. Phys. Lett.* **2004**, *393*, 51−57.
(46) Christiansen, O.; Koch, H.; Jorgensen, P. *Chem. Phys. Lett.* **1995**, *243*, 409−418.
(47) Verlet, L. *Phys. Rev.* **1967**, *159*, 98−103.
(48) Ponder, J. W.; Richards, F. M. *J. Comput. Chem.* **1987**, *8*, 1061.
(49) Jorgensen, W. L.; Maxwell, D. S.; Tirado-Rives, J. *J. Am. Chem. Soc.* **1996**, *118*, 11225−11236.
(50) Jorgensen, W. L.; McDonald, N. A. *J. Mol. Struct. Theochem* **1998**, *424*, 145−155.
(51) Jorgensen, W. L.; Ulmschneider, J. P.; Tirado-Rives, J. *J. Phys. Chem. B* **2004**, *108*, 16264−16270.
(52) Jorgensen, W. L.; Chandrasekhar, J.; Madura, J. D.; Impey, R. W.; Klein, M. L. *J. Chem. Phys.* **1983**, *79*, 926−935.
(53) Frisch, M. J.; ; et al. *Gaussian 09*, revision A.1; Gaussian, Inc.: Wallingford, CT, 2009.
(54) Inokuchi, Y.; Kobayashi, Y.; Ito, T.; Ebata, T. *J. Phys. Chem. A* **2007**, *111*, 3209−3215.
(55) Roshchupkin, D. I.; Talitsky, V. V.; Pelenitsyn, A. B. *Photochem. Photobiol.* **1979**, *30*, 635−643.
(56) Roos, B. O.; Taylor, P. R.; Siegbahn, P. E. M. *Chem. Phys.* **1980**, *48*, 157−173.
(57) Frisch, M. J.; Ragazos, I. N.; Robb, M. A.; Schlegel, H. B. *Chem. Phys. Lett.* **1992**, *189*, 524−528.